Status of Calibration and Data Analysis of MAXI GSC

Mutsumi Sugizaki,[1] on behalf of MAXI GSC Team,[12]

[1] RIKEN, [2] JAXA, Tokyo Tech., Aoyama Gakuin Univ., Nihon Univ.,
E-mail(MS): sugizaki@riken.jp

Abstract

Status of the instrument response calibration and the data analysis of MAXI/GSC are reviewed. Light curves and images of about 240 pre-registered X-ray sources are processed from the all-sky scan data every day. They are archived on the MAXI public web site (http://maxi.riken.jp). The spectra and response files for several major test sources have been open to public since October, 2010. Targets to be monitored and their archived products have been updated frequently according to the revision of the software and calibration files. The paper also briefly describes the GSC in-orbit performance and the expected scientific specification from the first-year operation.

Key words: instrumentation: detectors – X-rays: general – X-rays: individual (Crab Nebula)

1. Introduction

MAXI (Monitor of All-sky X-ray Image) is the first astronomical mission operated on the ISS (International Space Station) (Matsuoka et al. 2009). The GSC (Gas Slit Camera) is the main X-ray camera onboard MAXI, which covers the energy band from 2 to 30 keV using large-area Xe-gas proportional counters (Mihara et al. 2011). The total detector area becomes 5350 cm^2. The detectors with a position sensitivity and the slat collimators with a slit constitute slit camera optics. The six identical units cover two rectangular wide fields of views (FOVs) of $1.5^\circ \times 160^\circ$ pointed towards the earth-horizon and the zenith directions. The two FOVs enable to scan the entire sky every 92-minute orbital period even if some of the detectors have to be partly downed in a heavy irradiation environment such as the passage of the SAA (South Atlantic Anomaly). This paper presents the GSC in-orbit performance including the operation and calibration status (see also Sugizaki et al. 2011).

2. In-orbit Performance

2.1. HV Operation

Full GSC operation with twelve counter units, named as GSC_0, ..., GSC_9, GSC_A, GSC_B, started on August 15, 2009. The high voltages of all the twelve gas counters were set at the nominal 1650 V. They are reduced to 0 V when the ISS passes through heavy particle background area defined by an on-board Radiation-Zone (RZ) map. In the beginning of the mission, we set the RZ map only at the SAA. On September 8, 2009, the analog power on the GSC_6 counter was suddenly downed. It was followed by the power down of another counter, GSC_9, on September 14. The data indicate that a carbon-anode wire in each of these counters was fractured. It was also suggested that the location fractured on the carbon wire would be where a large amount of discharges occurred repeatedly. We then changed the counter operation strategy so that any risks to cause potential damages on the carbon-anode wire such as discharge and heavy irradiation should be avoided. The high-voltage reduction at the high latitude above 40° was employed since September 23. Two noisy counters, GSC_A and GSC_B, which are considered to be fractured sooner, were also tentatively stopped on September 26. On March 26, 2010, the analog power on the GSC_3 counter was downed, which were considered to be due to a carbon-wire fracture by breakdown discharge again. Since then, the operation voltage of counters with any discharge experience was reduced to 1550 V. These limited HV operation reduces the effective observation time to about 40% of that in the initial full operation. The sensitivity is expected to be reduced by a factor of three as discussed in § 2.5.. The three counters suffering from the breakdown will be soon activated with great care.

2.2. Particle Rate

GSC incorporates Radiation-Belt Monitor (RBM) to monitor the flux of the cosmic rays in orbit. Two silicon-PIN-diode detectors with 0.2-mm thickness and 5×5 mm^2 area are equipped with each of GSC horizon and zenith center units. The detector on the horizon unit (RBM-H) is faced to the tangential direction of the ISS motion along the earth horizon. The zenith unit (RBM-Z) is faced perpendicular to the horizontal plane. The RBMs always monitor count rates of cosmic rays with a certain energy deposit, whose threshold can be changed by commands. The level of the threshold is set at 50 keV, which corresponds to the half of the minimum ionization-loss energy of the relativistic particles.

Figure 1 shows the RBM count-rate maps on the ISS orbital area by RBM-H and RBM-Z units, respectively, averaged over the data taken for the first year. The two RBM rates agree with each other in the low count-rate area below 0.2 Hz, where the anti-correlations with the geomagnetic cutoff rigidity (COR) are seen clearly. It indicates that the origins are energetic cosmic rays. The cosmic-ray flux ~ 1 counts cm^{-2} s^{-1} and its relation with the COR are consistent with those obtained by ASCA (Makishima et al. 1996) and Suzaku (Kokubun et al. 2007) in low-earth orbit although the altitude of the ISS, 340–360 km, is different from that of these satellite, 530–590 km.

While the two RBM rates are agreed at the low radiation area, they are quite different in the high radiation area around the SAA and the both geomagnetic poles. The RBM-H rate is higher by an order of magnitude than the RBM-Z rate in these area. This is considered to be due to the anisotropy of the flux of trapped particles. A large number of cosmic-ray particles trapped by the geomagnetic fields are moving circularly on the horizontal plane around the magnetic pole. The RBM-Z detector faced on the zenith direction is insensitive to the particles moving on the horizontal plane. The anisotropy of the trapped particles at the high latitude has also been recognized by images of particle tracks taken by the SSC CCD imager (Tsunemi et al. 2010).

2.3. Background Spectrum

Figure 2 shows the GSC background spectrum normalized by effective area, and those of the Ginga LAC (Hayashida et al. 1989) and the RXTE PCA (Jahoda et al. 2006), where expected contribution of the CXB in each instrument are included. Crab-like source spectra are shown together as the comparison. The GSC background is approximately 2 mCrab at 4 keV and 10 mCrab at 10 keV. The level is almost comparable to that of the Ginga LAC and slightly higher than that of the RXTE PCA.

2.4. All-sky Exposure Map

Exposure maps on the sky for given periods are calculated from the counter HV-operation history, the detector effective area as a function of a photon incident angle, and information of the ISS orbit, attitude, and configuration parameters interfering the FOV such as the solar paddles, the space-shuttle vehicle docked on the ISS. Figure 3 shows the actual exposure maps by all operated GSC counters for 92 minutes of an ISS-orbital cycle, one day, and 27 days since January 2, 2010, 00:00 (UT), calculated from all the required information during these periods. GSC covers approximately 85% of the whole sky for one orbit except for the orbits including the SAA

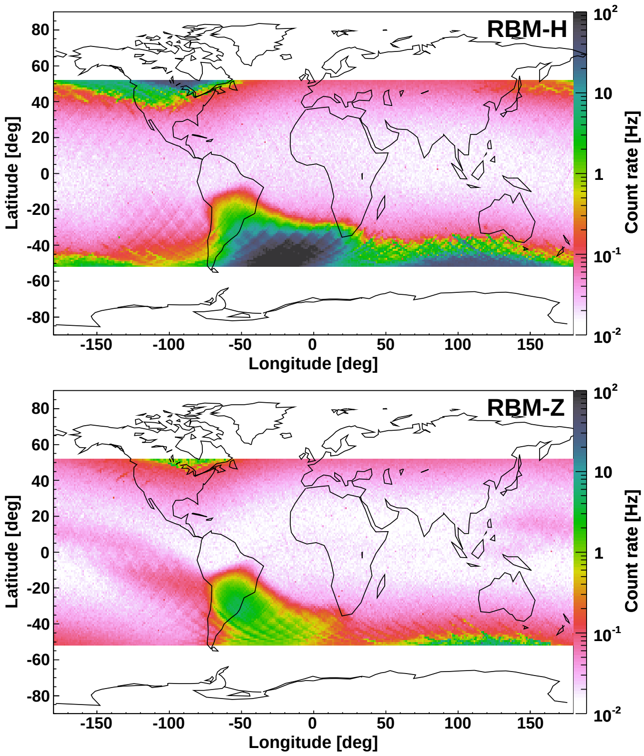

Fig. 1. RBM count-rate maps of horizon (RBM-H, top panel) and zenith (RBM-Z, bottom panel) units.

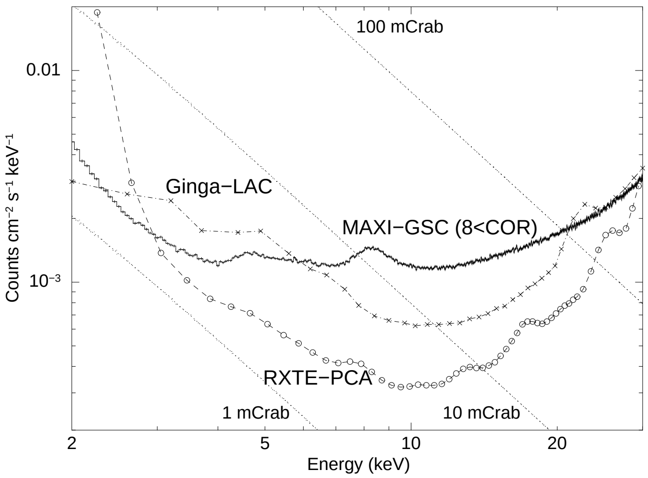

Fig. 2. GSC background energy spectrum normalized by effective area and comparison with those of Ginga-LAC, RXTE-PCA, and Crab-like source spectra. Expected contributions of the CXB in each instrument are included.

passage, and 95% for a day. The daily map has uncovered area for the Sun direction, the solar-paddle shadow, and the rotation pole that drift on the sky according to the precession of the ISS orbit. We can achieve the 100% full coverage in every three weeks.

2.5. Daily Effective Exposure for Celestial Targets

An exposure time for any celestial source on the sky during given observation period varies due to the change of scan direction according to the precession of the ISS orbit. Figure 4 shows the variation of the daily effective exposure for the Crab nebula since the operation start on August 15, 2009. It was typically $\sim$ 12,000 cm^{2}s during the first 1.5 month, then downed to $\sim$ 4000 cm^{2}s after four counters out of the twelve were stopped and the limited HV operation at the low latitude ($< 40^\circ$) was employed. It is expected to reduce the daily 5-σ source sensitivity to $\sim$ 15 mCrab, which is three times worse than that expected from the pre-flight simulation in the full operation (Matsuoka et al. 2009).

3. Calibration Status

3.1. Detector and Collimator Alignment

The attitude of the MAXI payload is continuously measured with the on-board Attitude Determination System (ADS), which consists of a Visual Star Camera (VSC) and a Ring Laser Gyroscope (RLG). Its accuracy is estimated to be better than an arc minute from the ground calibration tests. The source location of an incident X-ray on the sky is calculated from the position coordinates on the detector where the X-ray is absorbed and the attitude parameters at the event time. The alignments of the collimators and detectors on the payload module are calibrated using standard X-ray sources whose positions and intensities are well-known. The accuracy of 0.2° in the 90% containment radius of the best determined position has been confirmed so far using several bright-source samples selected randomly (Morii et al. 2011a).

3.2. Effective Area and Crab Light Curve

The visibility and the area of each GSC unit for a given X-ray source on the sky are always changing according to the ISS orbital motion and interferences with other relevant ISS activities, as described in § 2.4. and 2.5.. To derive the intrinsic time variation of a given X-ray source, the time-dependent effective area for the target has to be known. The light-curve response builder calculates the area curve of each GSC unit from the source coordinates, the ISS location, attitude, and the area of the GSC unit as a function of the source incident angle. The area of all the GSC units were calibrated on the ground using pencil X-ray beams (Morii et al. 2006).

Figure 5 shows the obtained light curve of Crab nebula in three energy bands of 2–4, 4–10, and 10–20 keV, respectively. Backgrounds are estimated from the count

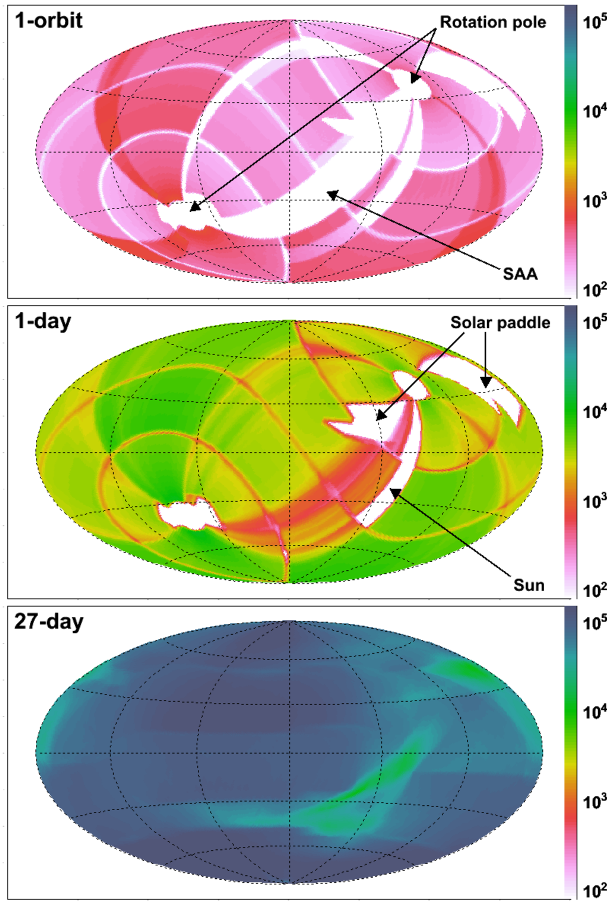

Fig. 3. GSC exposure map by scans of 92-minute orbital period (top), 1 day (middle), and 27 days (bottom) since 2010 January 2 00:00 (UT). The color scales of all three panels are identical and represent the effective exposure for the sky direction in the units [cm^{2}s]. The uncovered areas for the rotation pole, the Sun direction, the SAA, and the interference with the solar paddles are indicated with arrows.

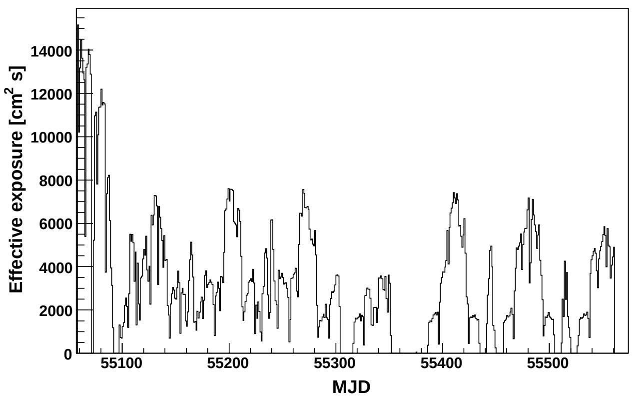

Fig. 4. Daily effective exposure for Crab nebula since the GSC operation start on August 15, 2010. It was typically $\sim$ 12,000 cm^{2}s during the first 1.5 month, then downed to $\sim$ 4000 cm^{2}s after the limited HV operation at the low latitude ($< 40^\circ$) was employed.

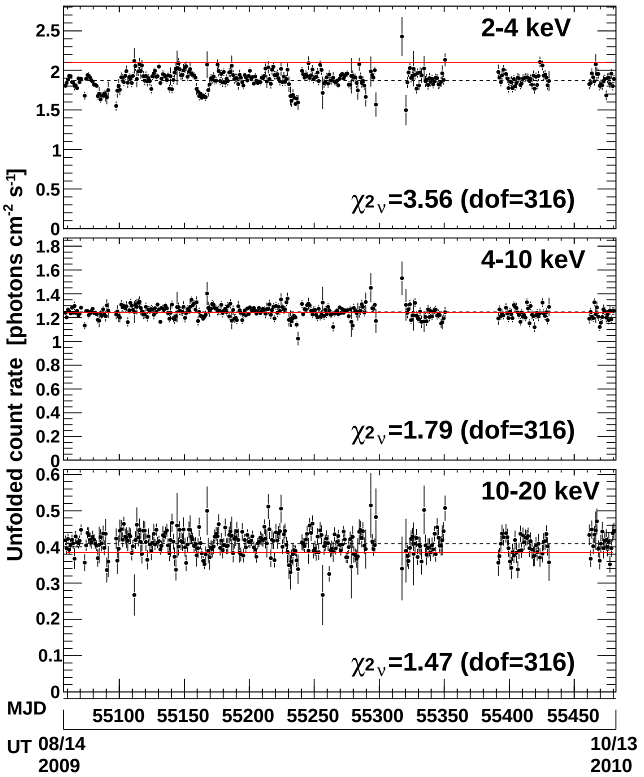

Fig. 5. Area-corrected light curves of Crab nebula in the three energy bands of 2–4 keV (top), 4–10 keV (middle) and 10–20 keV (bottom). Each data point represents the daily average flux corrected for the time-dependent effective area and the backgrounds. The vertical errors represent the 1-sigma statistical uncertainties. A power-law energy spectrum with a photon index, $\Gamma = 2.1$, is assumed in the effective-area correction. Solid lines represent the expected count rate from the standard Crab flux and dotted lines are the best-fit constant model. The best-fit reduced chi-square (χ^2_ν) and the degree of freedom (dof) are shown in each panel.

rates for the adjacent sky region, which corresponds to the data obtained in the successive time periods. A power-law energy spectrum with a photon index, $\Gamma = 2.1$, is assumed in the effective-area correction. These light curves should be approximately constant and consistent with the values expected from the standard Crab spectrum. The best-fit models with a constant and those expected from the standard Crab spectrum are shown together in the figure. Due to the inaccuracy of the effective-area calibration, these data show variations exceeding the statistical fluctuation and do not completely agree with the expected values within the errors. The errors on the corrected fluxes are estimated to be $-11\pm5\%$, $+0 \pm 3\%$, $+6 \pm 6\%$ with the 1-σ range in 2–4, 4–10, and 10–20 keV bands, respectively.

Table 1. Best-fit parameters for GSC Crab-nebula spectrum

Model	N_H[a]	Γ[b]	Norm.[c]	χ^2_ν (DOF)
Wabs*PL	0.72 ± 0.22	2.15 ± 0.05	11.4 ± 1.0	1.08 (43)
Wabs*PL	0.35: fix	2.08 ± 0.03	9.9 ± 0.4	1.25 (44)

All errors represent 90% conf. limits of statistical uncertainty.
[a] Absorption hydrogen column density in units of 10^{22} cm^{-2}.
[b] Power-law photon index
[c] Power-law norm. in units of photons cm^{-2} s^{-1} keV^{-1} at 1 keV.

3.3. Energy Response Matrix

The energy response matrix is represented by a product of the effective area and the dispersion relation between the incident X-ray energy and the PHA of the output signal. The dispersion relation as well as the gas gain depend on the 3-dimensional location where the X-ray photon is absorbed in a detector gas cell. The spatial gain variation and the time variation in orbit are corrected event by event in the first data-reduction process using calibration data collected from the ground and in-orbit test results. All the dispersion relations required to derive the response matrix were taken in the ground test (Mihara et al. 2002).

The energy response builder calculates the effective area and the energy redistribution matrix for a target source at given sky coordinates during a given observation period. The program accumulates instantaneous response functions for the source location according to the variation of the incident angle during the active observation period.

Figure 6 shows a Crab spectrum by GSC taken for a day on August 15, 2009 (UT) and the best-fit power-law model with an interstellar absorption, folded by the response matrix obtained by the response builder. Backgrounds are extracted from events in the adjacent sky region. The best-fit parameters are summarized in table 1. The model-to-data ratio shows that the obtained spectrum is well reproduced within 10% over the 2-30 keV energy range. The best-fit absorption column density, $0.72 \pm 0.22 \times 10^{22}$ cm^{-2} is slightly higher than the standard Crab value, 0.35×10^{22} cm^{-2} (Kirsch et al. 2005) although the fit with the absorption fixed at the standard value is also accepted within the 90% confidence limit. The discrepancy is considered to be in inaccuracy of the effective-area calibration at the low energy band. The fine calibration is in progress.

Figure 7 shows the variations of the best-fit parameters of the power-law model for daily Crab-nebula spectrum since August 15, 2009 (UT). They are mostly constant over the entire observation period except for some irregular periods. The detail calibration and the verification of the analysis processes applicable to all the observation periods are still in progress.

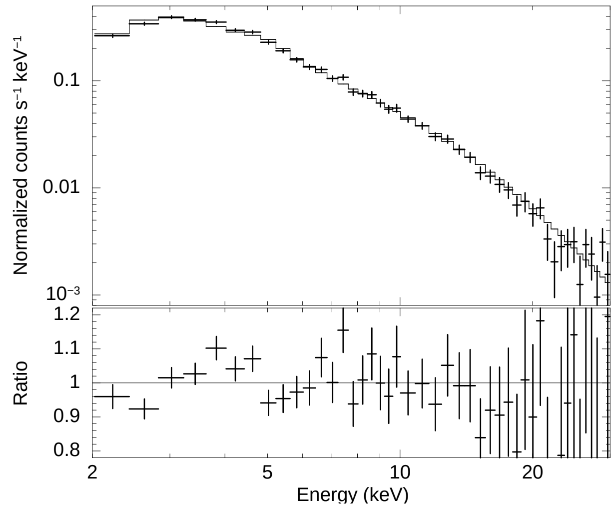

Fig. 6. GSC Crab-nebula spectrum taken for a day on August 15, 2009 (UT) and the best-fit power-law model with a fixed absorption of 0.35×10^{22} cm^2 (top). Data-to-model ratio (bottom).

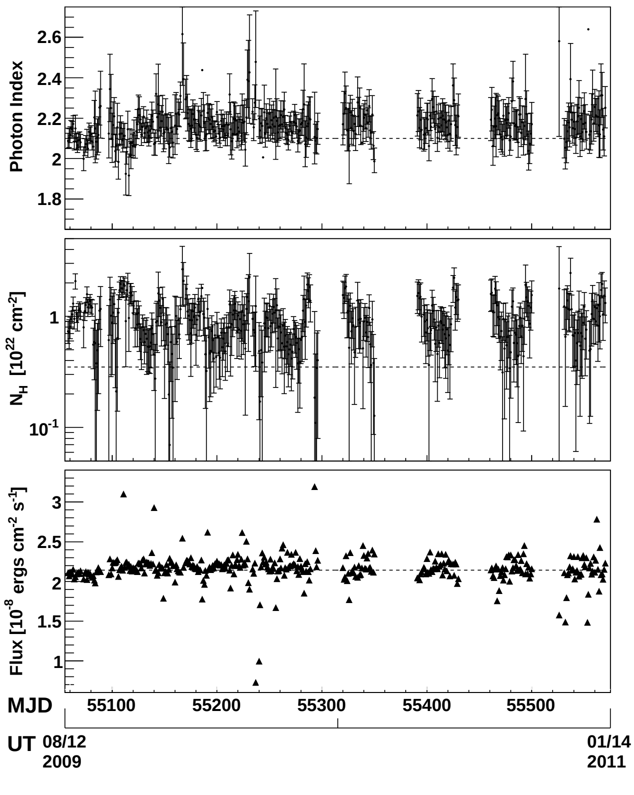

Fig. 7. Variations of best-fit parameters of absorbed power-law model for daily Crab-nebula spectrum: (top) power-law photon index Γ, (middle) absorption hydrogen column density N_{H}, (bottom) model flux in 2–10 keV band. Error bars in the top and middle panels show their 90% confidence limits of the statistical uncertainties. Dashed lines represent these values of the standard spectral model of Crab-nebula.

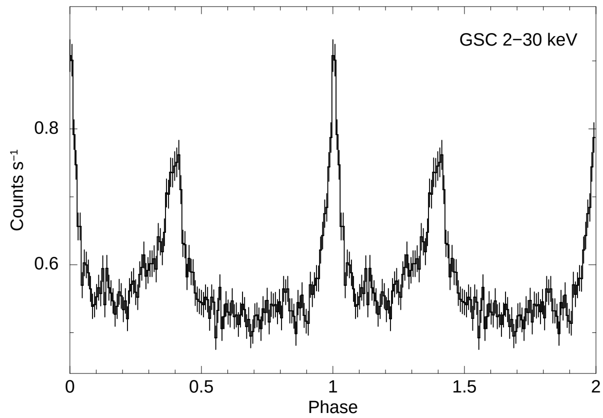

Fig. 8. Folded light curve of the Crab pulsar in 2–30 keV band obtained with GSC during a period from January 1 to January 5, 2010. The vertical count rate represents the event rate from the target direction over the entire elapsed period.

3.4. Timing

In-orbit timing calibrations are performed using signals from X-ray pulsars or binaries, such as Crab pulsar and Cen X-3 with 33 millisecond and 4.8 second period, respectively. Events within the PSF of these pulsars are extracted and applied to the barycentric correction. The pulsation of Crab pulsar can be detected for every one-day interval. Figure 8 show the folded pulse profiles since January 1 to January 5, 2010. The absolute timing and the relative stability are estimated by the relative pulse phase of the Crab pulsar to those with the radio wavelength (Lyne et al. 1993) and RXTE/PCA (Rots et al. 2004), and comparison of the Cen X-3 pulse period and phase with those of the Fermi/GBM (Meegan et al. 2009). We confirmed the timing stability of an order of 10^{-9} (See also Morii et al. 2011b).

4. Data Reduction and Analysis Process

Figure 9 illustrates the schematic of the MAXI data reduction and analysis flows. The system is same as those of other X-ray astronomical missions. We employ a relational-database system called MAXI-DB for the primary data storage in order to handle the all-sky data efficiently (Negoro et al. 2004). The database includes X-ray event data as well as auxiliary data, which collects various information regarding the environmental condition on ISS and the mission-operation status such as orbit and attitude parameters, configuration of the solar-battery panels, powers and temperatures of X-ray detector units, modes of the data processor, data of radiation monitors, and so on.

The calibration database are created from ground test data as well as in-orbit observation data. We use the HEASARC CALDB system to maintain the calibration

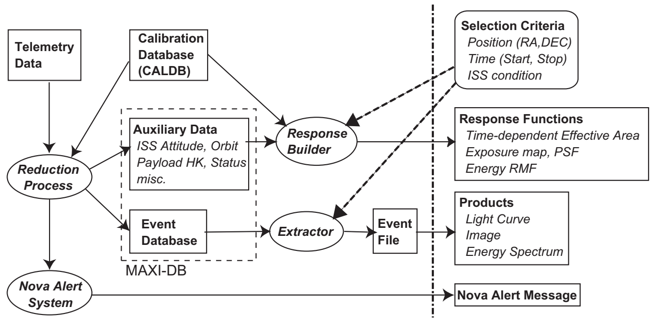

Fig. 9. Schematic of MAXI data reduction and analysis flows.

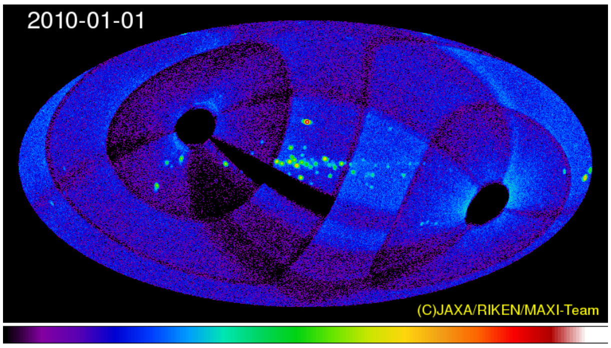

Fig. 10. Daily all-sky image by GSC taken on January 1, 2010

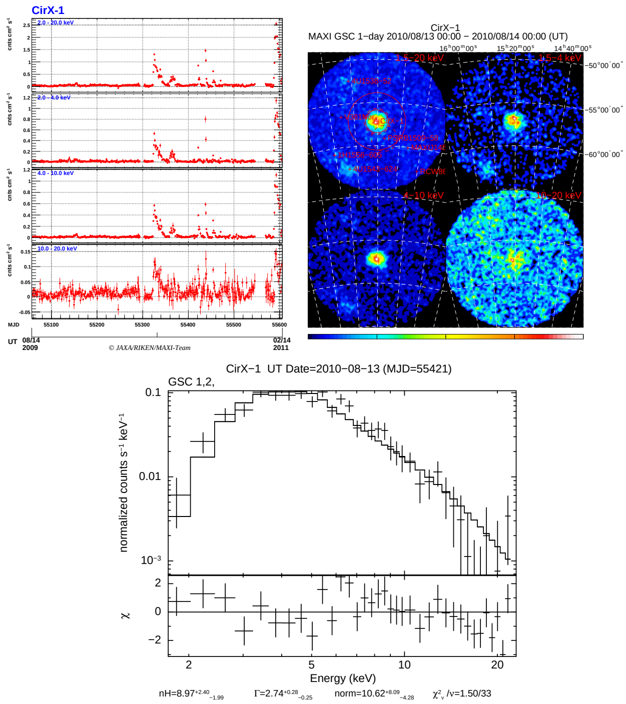

Fig. 11. Example of light curve (top lef), daily image (top right), and spectrum (bottom of pre-registered monitor targets archived on the MAXI web page (http://maxi.riken.jp) : in Cir X-1 case.

database. Some event-data parameters such as the photon arrival time, expected source position on the sky, and the energy, are calculated during the reduction process using the calibration data and the auxiliary data.

The science analysis of MAXI data starts with event selection for a target of interest from all-sky data. An event file for the target source is extracted from the event database. Light curves, images, and energy spectra for the target source are then created from the event file. The response files for these data products are also created with response builders in this step using the event-selection parameters.

5. Early Archival Data Products and Future Plan

We are developing a MAXI data-archive system so that any users can extract data of interest flexibly and analyze them easily. At the moment of January 2011, preliminary daily-data products which includes all-sky image, long-term light curves and images of pre-registered sources, spectra and response-matrix files of several test sources are open to public at the maxi web site at http://maxi.riken.jp. Figure 10 and 11 show their examples. The web interface for on-demand data archive will be opened when the initial instrument verifications are completed and the system is ready to release.

References

Hayashida, K., et al. 1989, PASJ, 41, 373
Jahoda, K., et al. 2006, ApJS, 163, 401
Kirsch, M. G., et al. 2005, Proc. SPIE, 5898, 22
Kokubun, M., et al. 2007, PASJ, 59, S53
Lyne, A. G., et al. 1993, MNRAS, 265, 1003
Makishima, M., et al. 1996, PASJ, 48, 171
Matsuoka, M., et al. 2009, PASJ, 61, 999
Meegan, C., et al. 2009, ApJ, 702, 791
Mihara, T., et al. 2002, Proc. of SPIE 4497, 173
Mihara, T., et al. 2011, PASJ, in press
Morii, M., et al. 2006, Proc. SPIE, 6266 6263U
Morii, M., et al. 2011a, Physica E: Low-dimensional Systems and Nanostructures, 43, 692
Morii, M., et al. 2011b, in this proceedings
Negoro, H., et al. 2004, Astronomical Data Analysis Software and Systems (ADASS) XIII, 314, 452
Rots, A. H., et al. 2004, ApJL, 605, L129
Sugizaki, M., et al. 2011, PASJ, in press
Tsumemi, H., et al. 2010, PASJ, 62, 1371
Turner, M. J. L., et al. 1989, PASJ, 41, 345